



# Glacier melting during lava dome growth at Nevado de Toluca volcano (Mexico): Evidences of a major threat before main eruptive phases at ice-capped volcanoes



L. Capra<sup>a,\*</sup>, M. Roverato<sup>b</sup>, G. Gropelli<sup>c</sup>, L. Caballero<sup>d</sup>, R. Sulpizio<sup>e</sup>, G. Norini<sup>c</sup>

<sup>a</sup> Centro de Geociencias, UNAM, Mexico

<sup>b</sup> Departamento de Geología Sedimentar e Ambiental (GSA), Instituto de Geociências (IGC), Universidade de São Paulo, São Paulo, SP 05508-080, Brazil

<sup>c</sup> Istituto per la Dinamica dei Processi Ambientali – Sezione di Milano, CNR, Milano, Italy

<sup>d</sup> Facultad de Ciencias, UNAM, Mexico

<sup>e</sup> Dipartimento di Scienze della Terra e Geoambientali, via Orabona 4, 70125 Bari, Italy

## ARTICLE INFO

### Article history:

Received 19 September 2014

Accepted 12 February 2015

Available online 21 February 2015

### Keywords:

Nevado de Toluca volcano

Glacier melting

Dome collapse

Block-and-ash flow deposits

Fluviatile sequence

## ABSTRACT

Nevado de Toluca volcano is one of the largest stratovolcanoes in the Trans-Mexican Volcanic Belt. During Late Pleistocene its activity was characterized by large dome growth and subsequent collapse emplacing large block and ash flow deposits, intercalated by Plinian eruptions. Morphological and paleoclimate studies at Nevado de Toluca and the surrounding area evidenced that the volcano was affected by extensive glaciation during Late Pleistocene and Holocene. During the older recognized glacial period (27–60 ka, MIS 3), the glacier was disturbed by the intense magmatic and hydrothermal activity related to two dome extrusion episodes (at 37 ka and 28 ka). Glacier reconstruction indicates maximum ice thickness of 90 m along main valleys, as at the Cano ravines, the major glacial valley on the northern slope of the volcano. Along this ravine, both 37 and 28 ka block-and-ash deposits are exposed, and they directly overlay a fluviatile sequence, up to 40 m-thick, which <sup>14</sup>C ages clearly indicate that their emplacement occurred just before the dome collapsed. These evidences point to a clear interaction between the growing dome and its hydrothermal system with the glacier. During dome growth, a large amount of melting water was released along major glacial valleys forming thick fluvio-glacial sequences that were subsequently covered by the block-and-ash flow deposits generated by the collapse of the growing dome. Even though this scenario is no longer possible at the Nevado de Toluca volcano, the data presented here indicate that special attention should be paid to the possible inundation areas from fluviatile/lahar activity prior to the main magmatic eruption at ice-capped volcanoes.

© 2015 Elsevier B.V. All rights reserved.

## 1. Introduction

Volcano–ice interaction has been the object of several studies, including perturbation of ice and snow by subglacial eruptions, geothermal activity, lava flows, pyroclastic flows and tephra fall on snow–ice surfaces (i.e. Major and Newhall, 1989; Guðmundsson et al., 1997), all processes driving to glacier melting and water discharge. Geothermal activity, sub-glacial eruptions, and pyroclastic flows emplaced on a snow–ice surface are probably the more effective processes in glacier melting with a rapid release of a large amount of water producing lahars (Major and Newhall, 1989). A dramatic example is the 1985 reawakening of Nevado del Ruiz volcano, where small pyroclastic flows melted part of the summit glacier inducing lahars that killed more than 20,000 people (Williams, 1987; Pierson et al., 1990). Supraglacial lava flows or tephra fall cannot melt ice or snow rapidly,

especially for thick layers (i.e. Rivera et al., 2006; Brock et al., 2007), but they still affect glacier activity, especially at low latitude stratovolcanoes, for example at Popocatepetl volcano, where the climatic-induced recession of the glacier between 1958 and 1998 was drastically accelerated due to the increase on tephra fallout in the summit area, which led to the total glacier consumption in 2004 (Julio-Miranda et al., 2008).

Examples of snow and ice perturbations reported in the literature demonstrate that before or during a magmatic eruption, ice–lava interaction can enhance the secondary effect that can generate lahars and floods with catastrophic effects (Major and Newhall, 1989; Tuffen, 2010). Depending on the dynamic of the event, the response of magma–ice interaction can be very short in time (i.e. Nevado del Ruiz) or can be more progressive (days, months or years). This paper presents a geological investigation on volcanoclastic deposits interpreted as due to recurrent discharge of sediment-laden water floods from melted glacier at Nevado de Toluca volcano (Mexico) during Late Pleistocene, when large lava domes (~1 km<sup>3</sup>) were growing on the glaciated summit

\* Corresponding author at: Centro de Geociencias, UNAM, Querétaro, Mexico.  
E-mail address: [lcapra@geociencias.unam.mx](mailto:lcapra@geociencias.unam.mx) (L. Capra).

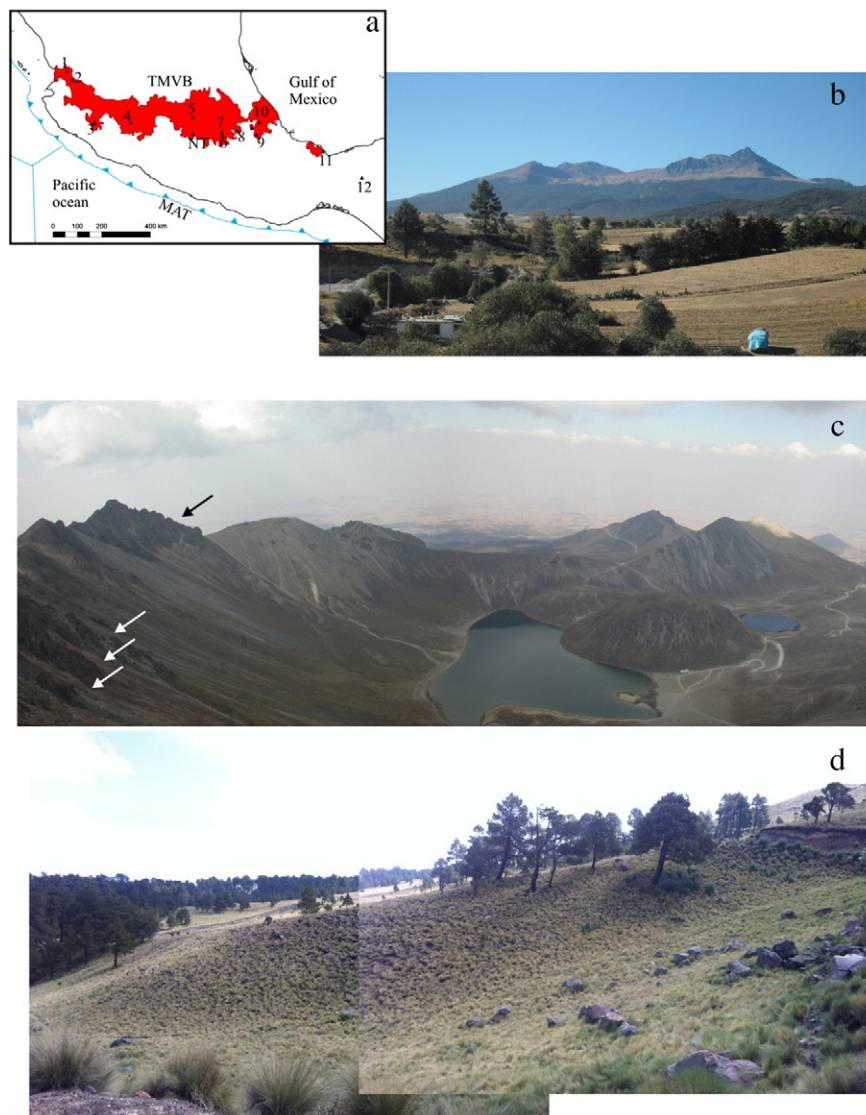
of the volcano. The sequence of the events here is based on stratigraphic correlations, lithofacies descriptions and radiocarbon ages. The glacier extension here is reconstructed for the Late Pleistocene, and stratigraphic correlations and  $^{14}\text{C}$  ages of both block-and-ash flow deposits and volcanoclastic deposits will be compared to demonstrate the link between volcanic activity and glacier perturbation in an ice capped volcano. Before this study, volcanoclastic successions at Nevado de Toluca volcano were mainly correlated with glacier retreat (Heine, 1988; Vázquez-Selem and Heine, 2011), instead of the magmatic activity of the volcano. At present the Nevado de Toluca is considered as a quiet volcano (Capra et al., 2008), and a glacier is no longer present at its summit (4680 m a.s.l.). However, the succession of events described here can represent a common scenario on ice capped volcanoes, which can have more catastrophic impact than the magmatic activity itself.

## 2. The Nevado de Toluca volcano: Late Pleistocene eruptive activity

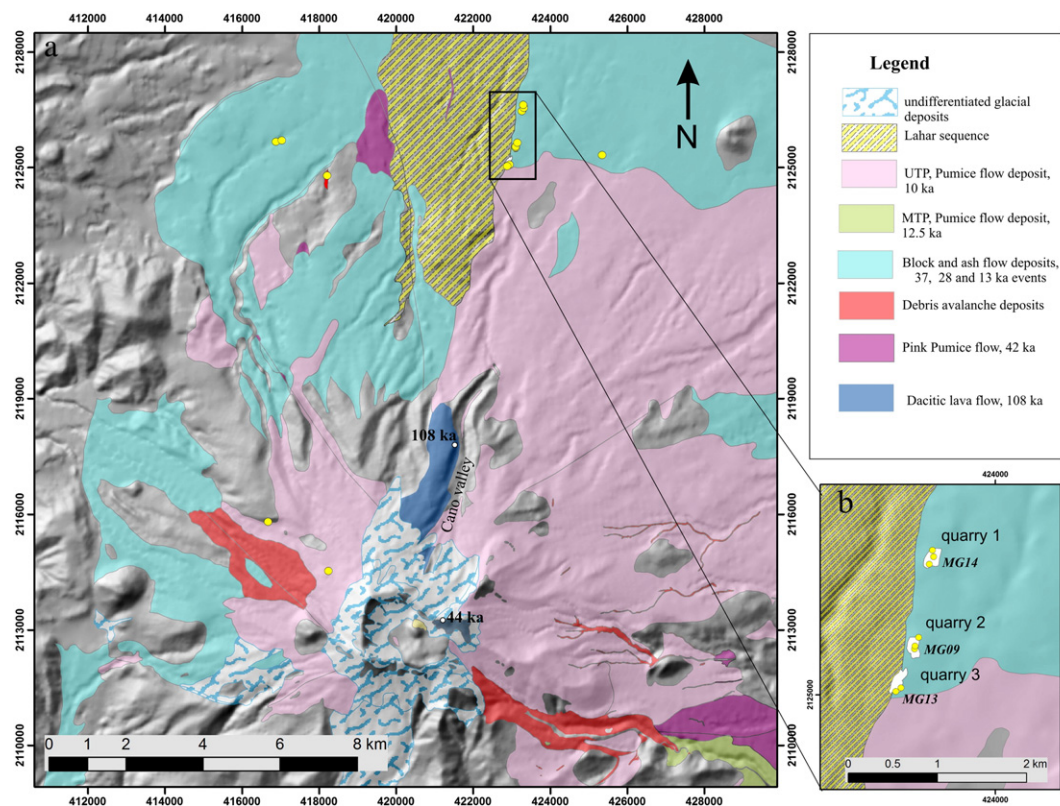
The Nevado de Toluca volcano (4680 m a.s.l.) is located in the central sector of the Trans-Mexican Volcanic Belt (Fig. 1a). It presents an elongated crater ( $1.8 \times 1.5$  km), occupied by two lakes separated by

the Ombligo dome. The volcanic edifice shows a gentle slope modified by several glaciations (Fig. 1b and d) (Heine, 1988). Its eruptive history can be subdivided into two main phases: (1) Between 1.5–1.3 Ma and 108 ka BP, with emplacement of voluminous andesitic and dacitic lava flows that built up the volcano edifice (Macías et al., 1997; García-Palomo et al., 2002; Bellotti et al., 2006; Torres-Orozco, 2012; Fig. 2); and (2) at ~42 ka BP ( $42,030 \pm 3000$   $^{14}\text{C}$  year BP,  $41,707\text{--}50,000$  cal year BP, Table 1) an explosive phase began, with alternating Plinian eruptions and central lava dome extrusions with subsequent collapse producing block-and-ash flow (BAF) deposits (Fig. 1b) (Macías et al., 1997; García-Palomo et al., 2002). Sector collapses were also recognized during this stage (Norini et al., 2008; Caballero and Capra, 2011). This explosive phase has probably started before, as stratigraphic evidences of older pyroclastic deposits are available, although dating of these deposits is not currently available.

Several papers on eruptive history of the volcano have been published, describing the volcanology of the major explosive events (e.g. Arce et al., 2003, 2005; D'Antonio et al., 2008). They include the 10.5  $^{14}\text{C}$  ka BP Upper Toluca Pumice Plinian eruption that erupted more



**Fig. 1.** (a) Sketch map of the Trans-Mexican Volcanic Belt where the Nevado de Toluca volcano and other main stratovolcanoes are located: (1) San Juan; (2) Ceboruco; (3) Colima Volcanic Complex; (4) Tancitaro; (5) Jocotitlán; (6) Popocatepetl; (7) Ixtacchuatl; (8) La Malinche; (9) Pico de Orizaba; (10) Cofre de Perote; (11) San Martín; and (12) Chichón. (b) Panoramic view of the volcano from the east. (c) Panoramic view of the interior of the crater of the volcano, showing the two lakes separated by the Ombligo dacitic dome, and where it is possible to distinguish relicts of the summit domes that now form the crater. Arrows point to dikes and dome remnants. (d) Picture showing one of the best defined moraine easily recognizable on the volcano slope.



**Fig. 2.** (a) Simplified geological map of the Nevado de Toluca volcano showing the distribution of the pyroclastic deposits associated with the last ~42,000 years of activity. Yellow dots represent stratigraphic sections discussed in the text. (b) Zoom of the studied area indicating the areal extension of the quarries where stratigraphic sections were studied.

than 8 km<sup>3</sup> of magma (DRE). The volcano was also the focus of several studies of tephrochronology (Metcalf et al., 1991; Caballero et al., 2000), pedostratigraphy (Solleiro-Rebollero et al., 2004) and glacial stratigraphy (Heine, 1988; Vázquez-Selem and Heine, 2011) aimed at the reconstruction of paleoclimate and environment during Late Pleistocene and Holocene. The only effort to correlate the paleoclimate and the volcanic activity was recently published to define the climatic factors that induced the edifice failure which occurred at 28 <sup>14</sup>C ka BP (Capra et al., 2013).

### 2.1. Central dacitic dome growth and block-and-ash flow deposits

During Late Pleistocene and Holocene the Nevado de Toluca volcano was characterized by large eruptions, dominated by the emplacement of BAF deposits from dome collapses, some of them accompanied by partial sector collapse, and at least four Plinian eruptions and associated pyroclastic density current (PDC) deposits. Fig. 2 shows the distribution of main BAF deposits recognized at Nevado de Toluca volcano (Norini, 2006; Capra et al., 2008). These deposits are grouped into a single stratigraphic unit, since they are very similar in texture and composition, and it is not always easy to distinguish between different events at an outcrop scale. Calibration of <sup>14</sup>C dating reported here was performed using the CALIB 5.0 program (Stuiver and Reimer, 1993), and the 2σ

range is reported in calibrated years before present (cal year BP) based on the calibration curve IntCal04 (Reimer et al., 2004) (Table 1). Two central dacitic dome growth episodes were recorded around 37 ka (37,000 ± 1125 <sup>14</sup>C year BP, 39,420–43,507 cal year BP) and 28 ka (28,925 ± 600 <sup>14</sup>C years BP, 31,250–34,459 cal year BP) based on the age obtained from charcoal collected in the BAF deposits (Macías et al., 1997). Only for the older event a <sup>40</sup>Ar/<sup>39</sup>Ar age of 44 ka is available for a lava dome on the crater (Fig. 2; Torres-Orozco, 2012). Based on the textural evidences of these PDC deposits, they were hypothesized as due to gravitational collapses of the summit central domes (Macías et al., 1997). The deposits are radially distributed and best crop out on the gentle slopes surrounding the volcano. The 37 ka deposit consists of three main flow units, up to 30 m in thickness; main components are poorly-vesicular, light gray dacitic lava fragments, red oxidized accidental lithics and pumices. The 28 ka deposit consists of at least three flow units with interbed of dilute PDC deposits and abundant gas pipes; main components are highly vesicular, gray dacitic lava fragments, pumice fragments and red oxidized accidental lithics. The 28 ka BAF deposit was preceded by the emplacement of a debris avalanche deposit, described in the eastern sector of the volcano (Caballero and Capra, 2011) and in the NW sector (Bellotti, 2004). Macías et al. (1997) estimated a volume of 16 km<sup>3</sup> for the block-and-ash flow deposits for both eruptions (28 ka and 37 ka), considering an

**Table 1**

<sup>14</sup>C ages of block-and-ash deposits and fluvialite sequences.

Sample	<sup>14</sup> C yrs BP	Calibrated <sup>14</sup> C yrs BP (2σ)	Reference
MG14	38,150 ± 410	41,992–43,240	This work
MG09	29,030 ± 170	34,460–33,180	This work
NT9595/42 ka, PPF <sup>a</sup>	42,030 ± 3000	41,707–50,000	Macías et al. (1997)
NT9550/37 ka, BAF <sup>a</sup>	37,000 ± 1125	39,420–43,507	Macías et al. (1997)
NT9521/28 ka, BAF <sup>a</sup>	28,925 ± 600	31,250–34,459	Macías et al. (1997)

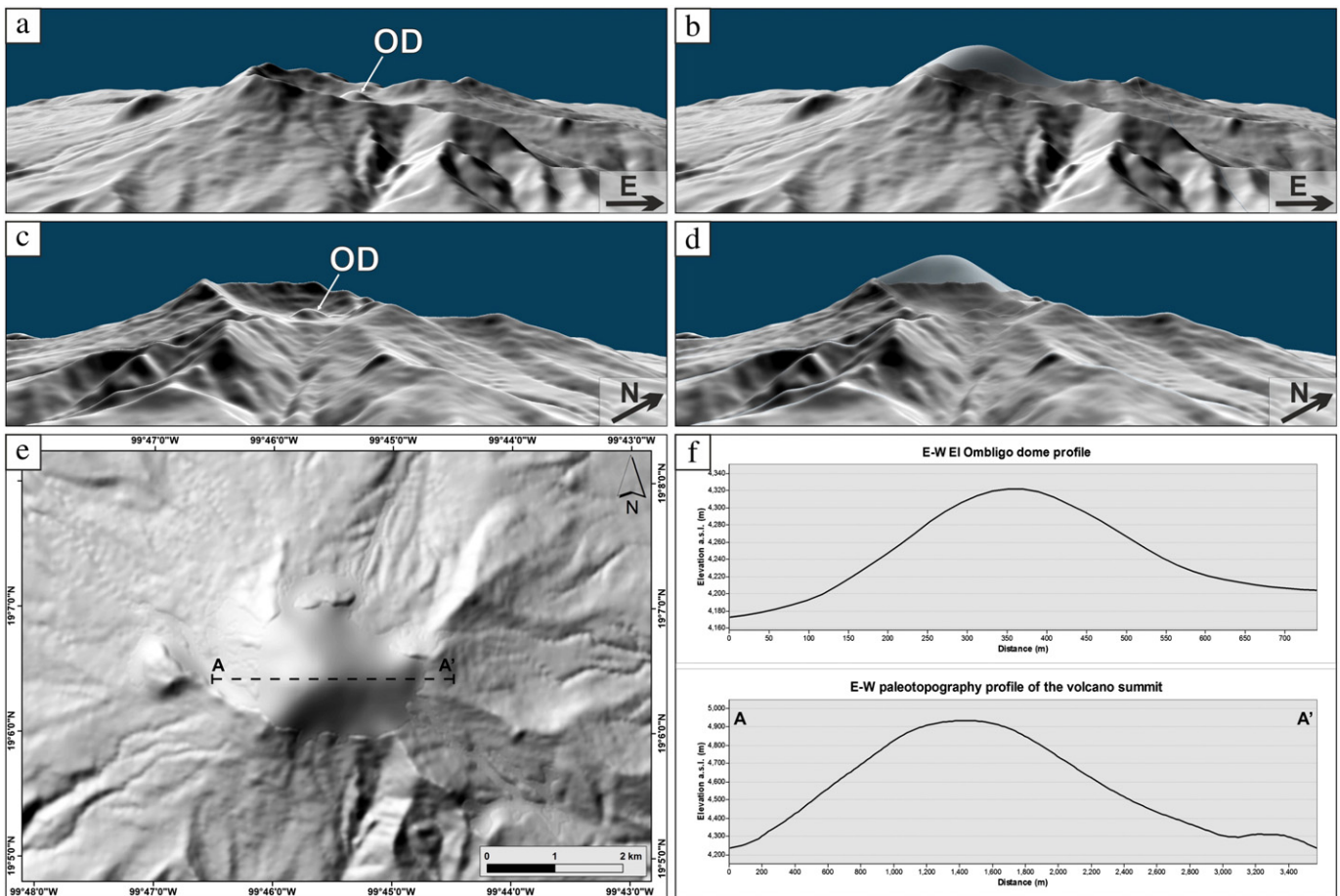
<sup>a</sup> Deposit names have been reported in previous works only based on their ages.

average thickness of 10 m radially distributed around the volcano and up to 14–16 km from the crater (Fig. 12 in Macías et al., 1997). Based on this estimation, and considering that the collapsed material expanded at least 30% (Wadge et al., 1995), the total volume of the extruded lava domes was  $\sim 11 \text{ km}^3$ , so  $\sim 5 \text{ km}^3$  for each dome. In the following section the summit dome morphology is reconstructed and new volume estimation is proposed.

### 3. Paleotopography and volume of the summit dome complex

The endogenous lava dome remnants that crop out in the crater area consist of massive, highly crystalline dacitic lavas with plagioclase crystals up to 1 cm. The lava flows are highly fractured, and some dikes are visible cutting previous lava bodies (Fig. 1c). The most recent lava dome inside the crater is the El Ombligo dome, a 90 m-high, well-preserved endogenous dome, surrounded by a thick blocky talus, which was extruded after the Upper Toluca Pumice Plinian eruption (Arce et al., 2003) (Fig. 1c). The crater was shaped by the interplay between the failure/explosive removal of the lava domes in the crater area and the tectonic/volcanotectonic activity in the edifice interior (Norini et al., 2008). To better understand the source of the block-and-ash flow deposits originated from the failure of the summit dome complex, we estimated the missing volume in the crater area. Perspective views of the shaded relief image of the present day Nevado de Toluca summit show that the pre-crater morphology of the volcanic cone is well preserved on its northern, western and southern flanks (Fig. 3a, c). Also, the summit lava dome remnants show the same lithology and structure of the well-preserved El Ombligo dome, so that we assume similar rheology,

endogenous regime and aspect ratio for the lava domes emplaced before the formation of the present-day crater and the El Ombligo dome. This allows reconstructing the morphology of the summit area inside the present-day crater rim, through the interpolation of elevation data of the topographic surface outside the crater, following the curvature and aspect ratio of the El Ombligo dome. A Digital Elevation Model (DEM) of the present day topography (20 m horizontal resolution) was used. We interpolated the elevation data of the DEM for several reference points located on the surface of the lava dome remnants around the crater by *regularized spline with tension* in a GIS (e.g. Mitasova and Hofierka, 1993; Mitasova and Mitas, 1993; Calvari et al., 2004; Norini et al., 2010). The interpolation tool was used to calculate the paleotopography of the volcano summit, on the assumption that it should pass through the reference points and should be at the same time as smooth as possible. A best-fitting of the interpolation parameters has also been performed to search for the interpolated surface that best resemble the aspect ratio and shape of the El Ombligo dome (Fig. 3f). The reconstructed paleotopography of the summit dome complex shows that it could have reached a maximum height of  $\sim 4950 \text{ m a.s.l.}$  (Fig. 3b, d, e, f), with an assessed volume of  $\sim 1 \text{ km}^3$ . This measure of the missing volume of the summit dome complex is considerably lower with respect to the value ( $5 \text{ km}^3$ ) estimated by previous authors and based on the BAF volume (Macías et al., 1997). A possible explanation that can partly account for this discrepancy is that several domes were continuously growing and collapsing over time, filling main ravines, where up to three flow units can be distinguished, or that the magmatic component contributed to increase the volume of the erupted material.



**Fig. 3.** Reconstruction of the morphology of the summit dome complex. Perspective views of the summit area from S (a) and from SE (c), where the Ombligo dome is visible. (b) and (d), perspective views of the reconstructed dome. (e) Shaded relief of the Nevado de Toluca morphology with the reconstructed summit dome, and the trace of the topographic profile A–A' of the reconstructed dome compared with the topographic profile of the Ombligo dome (f).

#### 4. Glacial stratigraphy at Nevado de Toluca: reconstruction of the glacier during Late Pleistocene

Heine (1988, 1994) and Vázquez-Selem and Heine (2011) reconstructed the glacial stratigraphy at Nevado de Toluca by mapping major moraines and rock glaciers and obtaining their ages based on  $^{36}\text{Cl}$  dating and tephrostratigraphy. For Mexico, Quaternary glacier stages have been recognized on main stratovolcanoes of the Trans-Mexican Volcanic Belt. Deposits correlated to the Marine Isotope Stage 6 (MIS 6, 205–175  $^{36}\text{Cl}$  ka, Vázquez-Selem and Heine, 2011) have been identified on the Iztacihuatl volcano, but only younger glaciation deposits were recognized in other volcanoes. The morphology of the Nevado de Toluca volcano shows evidence of extensive glaciations and several glacier advances were recognized by Vázquez-Selem and Heine (2011): >32  $^{14}\text{C}$  ka (MI), 21.7–17  $^{14}\text{C}$  ka (MII 1), 17–11.6  $^{14}\text{C}$  ka (MII 2), <11.6  $^{14}\text{C}$  ka (late Younger Dryer), 8–7  $^{14}\text{C}$  ka (MIV) and the Little Ice Age (MV). The MI episode correlated with well-defined moraines that are easily recognizable on all the W, N, and E flanks of the volcano (Figs. 1d and 4), up to an altitude of 3500 m a.s.l. In the present paper we will focus on this older glacial stage recognized on the Nevado de Toluca volcano, since it corresponds with the time span of the dome growth and collapse at 37 ka, as described in the previous sections. In addition reworked till and gelifluction deposits are also reported at >25  $^{14}\text{C}$  ka (Vázquez-Selem and Heine, 2011) so it is possible that the MI period

was even younger corresponding with the Marine Isotope Stage 3 episode (MIS 3, 27–60 ka), the pre-Last Glacial Maximum ice advance, as recently recognized in North America (Thackray and Staley, 2014), and suggested in the southernmost South America (Kaplan et al., 2008). Under this scenario, both 28 ka and 37 ka dome growth occurred when the volcano was ice-capped.

Based on the extension and spatial distribution of the moraines correlated with the MI glacial stage, the glacier extent and thickness were reconstructed with the methodology proposed by Benn and Hulton (2010) (Fig. 4a). With this aim, a 20 m resolution DEM was used to trace several topographic profiles along the main glacial valley between moraines and up to their maximum extent. To reconstruct the surface profile of the glacier, a glacier ice density of  $900\text{ kg/m}^3$  and a basal shear stress of 80 kPa were considered (i.e. Thorp, 1991; Benn and Hulton, 2010). The estimation was performed at each 100 m of distance along selected profiles. Fig. 4a shows the result obtained for the north-western sector of the volcano. It is worth mentioning that the present morphology of the crater is attributed to the Upper Toluca Pumice Plinian eruption, so the paleomorphology of the volcano summit before the initial stage of domes growth is unknown. A major explosive eruption occurred at 42 ka (Pink Pumice Flow unit, Macías et al., 1997), so it could be possible that prior to the 37 ka dome emplacement the volcano was characterized by an open crater. This hypothesis implies that the crater was also filled with ice prior to the dome extrusion, with variable thickness depending on the crater floor depth that is difficult to estimate. Based on this reconstruction, a total area of  $35\text{ km}^2$  of ice was covering the NNW sector of the volcano with maximum glacier thickness of up to ~90 m (Fig. 4b). The Cano ravine represents the more prominent glacial valley (Figs. 2 and 4). Its western flank consists of a dacitic lava flow dated at 108 ka BP (Torres-Orozco, 2012), which is deeply incised with a depth of more than 100 m.

#### 5. Stratigraphic reconstruction of the fluvial/pyroclastic succession

The best outcrops at Nevado de Toluca volcano are in quarries where deep excavations provide a better exposure of the pyroclastic successions. For the fluvial succession a lithostratigraphic description is used here (Fig. 5) in order to better illustrate vertical and lateral variability. Along the Cano ravine three different quarries were analyzed, labeled 1, 2 and 3 (Fig. 2). Section MG14 represents a composite section at quarry 1, 13 km from the crater (Figs. 6 and 7). The paleotopography is represented here by the 42  $^{14}\text{C}$  ka Pink Pumice Flow (PPF) deposit (García-Palomo et al., 2002), easily recognizable for the abundance in clay mineral in the matrix and a high degree of alteration that gives it a pink-orange color (Fig. 7f). The bottom of the quarry consists of a 10 m-thick succession of conglomerate units (lithofacies csCP, Fig. 5) alternating with thin hyperconcentrated flow deposits (lithofacies dsSst, Fig. 5). No evidences of paleosols have been recognized along the succession, suggesting it was deposited from a long-lasting fluvial system characterized by variations in flow energy. A 12 m thick BAF deposit overlies the succession (Figs. 6 and 7). The deposit consists of three main flow units. Each unit contains angular dacitic fragments, from few centimeters up to 70 cm in diameter, with centimeter pumice fragments and accidental cm-sized clasts. Thin sections from the juvenile dacitic lava fragment show mineralogical assemblage dominated by plagioclase, hornblende crystal with oxidized rims, rare orthopyroxene and xenocrystals of quartz, imbedded in a microcrystal ground mass. Humic organic material was collected between the two successions, and yields a  $^{14}\text{C}$  age of  $38,150 \pm 410$  year BP ( $41,992\text{--}43,240$  cal year BP, Table 1) (Fig. 7).

At quarry 2 (12 km from the crater), the stratigraphic succession is more complex (Figs. 8 and 9). At the bottom of the quarry, the first unit that crops out is a pumice fall deposit, 1.5 m thick, containing cm- to dm-size white pumices (Fig. 9b and c). The upper 40 cm of the deposit consists of reworked ochre pumice rich layers. A ~40 m-thick succession of debris flows (lithofacies mCSst, Fig. 5) and fluvial layers

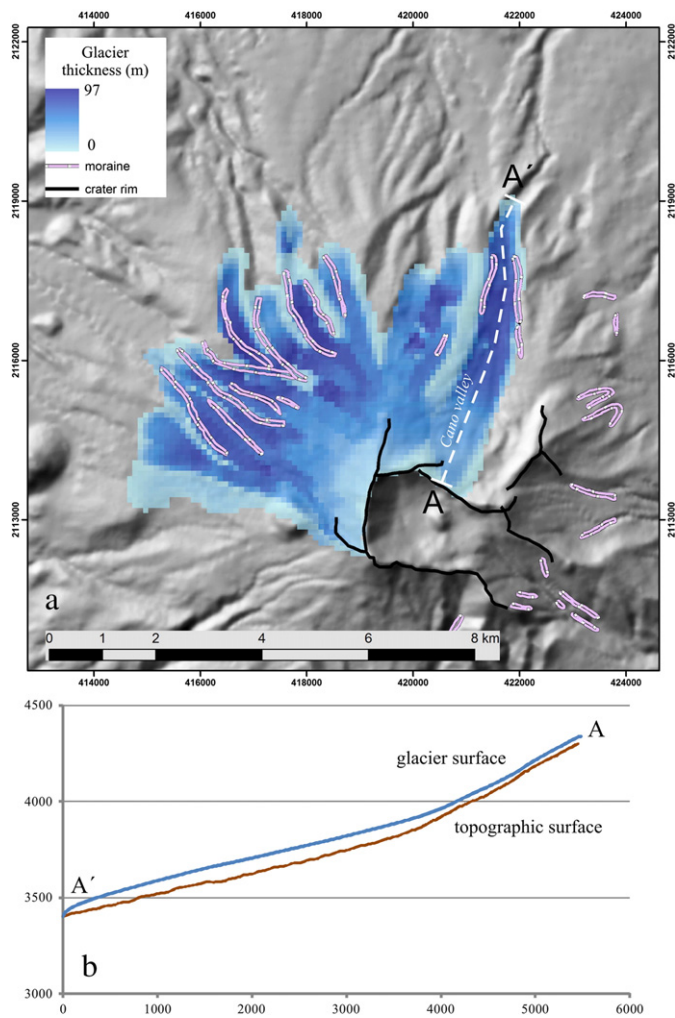

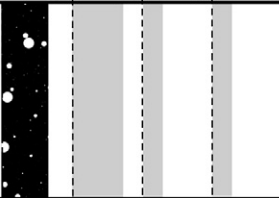



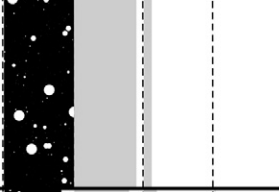

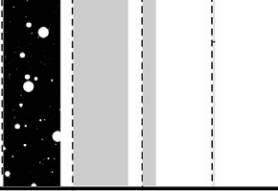


Fig. 4. (a) Distribution of the moraines (Heine, 1994) possibly correlated with the MSI 3 episode (60–27), that was used to reconstruct the glacier extent for this episode. (b) Topographic profile along Cano valley showing the glacier thickness obtained using the method proposed by Benn and Hulton (2010).

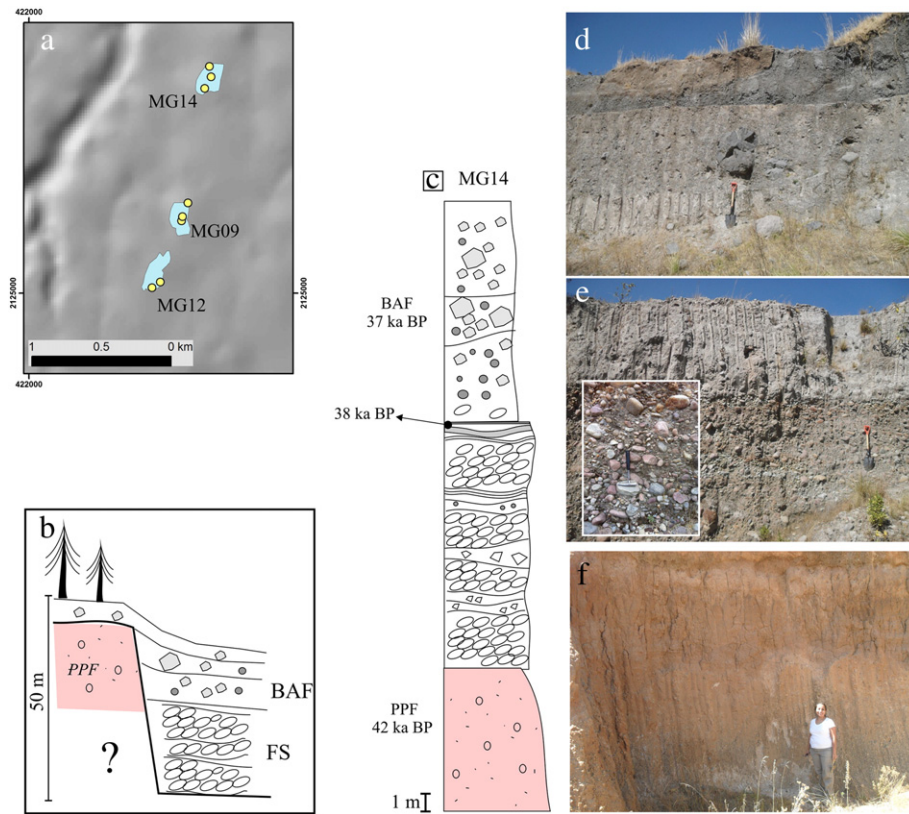
Lithofacies description			matrix size				
			wt%	wt%			
			matrix %	sand	silt	clay	
			0	1000	1000	1000	10
	<i>mCSSt</i>	Massive, matrix -supported, with sub-rounded cobble, dacitic in composition. Sandy matrix with 3% in clay. Individual layers are up to 1.5 m in thickness. Poor sorting.					
	<i>csCP</i>	Clast-supported, cobble to pebble, dacitic in composition, sandy matrix (> 10%) with 4% in clay. Oblate clasts show imbrication. Single layer thickness range between 1 and 2 m. Poor sorting.					
	<i>sSSt</i>	Stratified sand and < 10 % of silt, with lenses of cm-size rounded pumices. Individual laminae are discontinuous and truncated. Thickness of individual lenses range between 1-3 cm. Well sorting.					
	<i>dsSSt</i>	Crudely to diffusely stratified sand and < 20% of silt fraction. Pebbles form bedding surfaces. Thickness of individual lenses range between 1-10 cm. Medium sorting.					

The first letter of the code indicate the general appearance of the deposit (m = massive, cs = clast supported, xs = cross-stratified, ds = diffusely stratified) and capital letter indicate the grain size (P = pebble, C = cobble, S = sand, St = silt). Granulometric analyses of the matrix fraction (< 2 mm) were performed with a photosedimentograph Analysette-20.

Fig. 5. Facies description used along the text for the volcanoclastic sequence.



Fig. 6. Panoramic view of quarry 1, where it is possible to observe the horizontal contact between the fluvio-glacial sequence and the block-and-ash flow deposits at the top. The black arrow points to the contact.



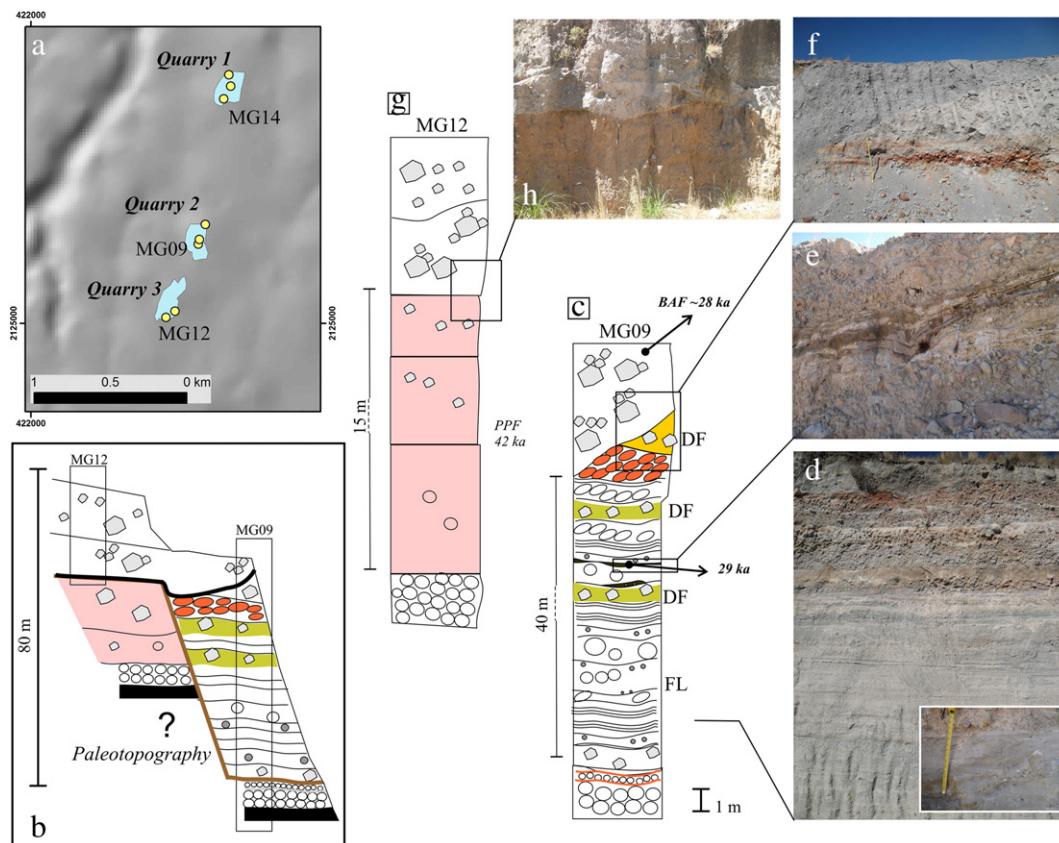
**Fig. 7.** Stratigraphic section MG14 at quarry 1. (a) Location of the studied section; (b) sketch of the stratigraphic relationship at this location, showing as the Pink Pumice Flow (PPF) deposit represents the paleotopography. (c) Composite stratigraphic section showing the abrupt contact between the conglomeratic sequences and the block and ash flow sequences. Organic material collected at the contact gives a  $^{14}\text{C}$  age of  $38,150 \pm 410$  years ( $41,992\text{--}43,240$  cal BP). The pyroclastic sequence is correlated here with the  $37,000 \pm 1125$  years ( $39,420\text{--}43,507$  cal BP) block-and-ash flow deposit (Macías et al., 1997); (d) picture showing the three flow units that compose the block-and-ash flow deposit; (e) contact between the pyroclastic unit on top of the conglomeratic unit. The inset shows the texture of the epiclastic deposit; (f) the PPF deposit that constitutes the paleotopography of the paleo-valley in which the younger sequence emplaced. FS: Fluvial sequence.

(lithofacies sSst and dsSst, Fig. 5), overlays the pumice fall deposit (Figs. 8b and 9d). This fluvial succession gradually changes into two massive debris flow deposits, up to 1.5 m in thickness (lithofacies mCSst, Fig. 5). Between these two deposits, a sandy fluvial layer is observable (lithofacies sSst, Fig. 5), forming the base of a ponded structure, probably representing a small puddle, where abundant organic material accumulated. This organic material was dated at  $29,030 \pm 170$   $^{14}\text{C}$  year BP ( $34,460\text{--}33,180$  cal year BP) (Fig. 9c and

e). The succession follows with 1.5 m-thick conglomerate (lithofacies csCO, Fig. 5) that shows here a high degree of oxidation toward the top. The reddish conglomerate is then directly overlain by a massive debris flow deposit (lithofacies mCSst, Fig. 5), up to 2 m thick. Both conglomerate and debris flow deposits are overlain by a pyroclastic unit in a sharp erosive contact (Fig. 9f). The pyroclastic unit consists of at least two flow units, with abundant gray, dacitic fragments, up to 10–15 cm in diameter.



**Fig. 8.** (a) Panoramic view of quarry 2 and (b) detail of the basal portion of the sequence dominated by fluvial horizons.



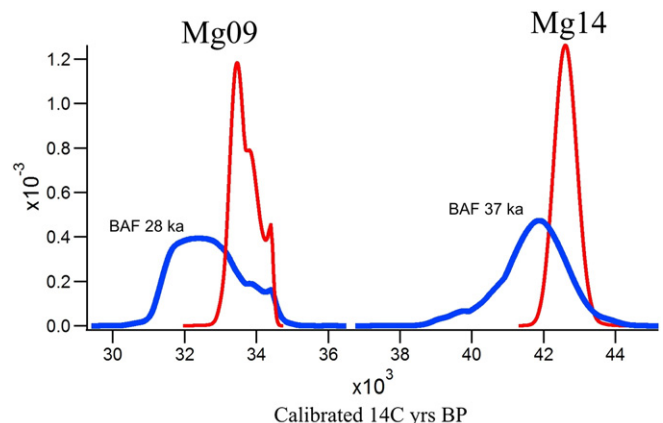
**Fig. 9.** Composite stratigraphic sections MG09 and MG12, respectively at quarry 2 and 3. (a) Location of the studied sections; (b) sketch of the stratigraphic relationship at these locations; (c) composite stratigraphic section at quarry 2 showing the 60 m-thick epiclastic sequence with the intercalation of fluviatile and conglomeratic horizons. The pyroclastic units are erosively overlaying the fluvio-glacial sequence. (d) Picture of the basal sequence, the inset is a detail showing the texture of the fluviatile sequences. (e) Picture of the upper portion of the fluvio-glacial sequence showing the layers rich in organic material that was dated at 29,030 years BP; (f) picture showing the erosive contact between the basal sequence and the upper pyroclastic unit; (g) composite stratigraphic section at quarry 3 where the upper pyroclastic sequence is directly on top of the 42 ka PPF that is forming the paleotopography here (h).

At quarry 3 the upper portion of this described sequence is still observable (MG12, Fig. 9g and h). Here the 42 ka PPF deposit is forming the paleotopography over which the upper sequence was emplaced (Fig. 9b, g and h). The upper portion of the sequence consists of two pyroclastic flow units. The basal layer consists of a chaotic deposit, up to 1.5 m in thickness, with abundant dark-gray dacitic lava fragments, variable in size from cm to dm, mostly concentrated forming domains where jigsaw-like features are observable. The upper unit, up to 2-m in thickness, consists of massive block-and-ash flow deposit with gray dacitic lava fragment imbedded in a sandy matrix. Pumice fragments are also observable. Thin sections from the juvenile dacitic lava fragment show mineralogical assemblage dominated by plagioclase, highly oxidized hornblende, orthopyroxene and quartz and biotite, imbedded in a microcrystal ground mass.

## 6. Discussion: glacier perturbation by central dome growth

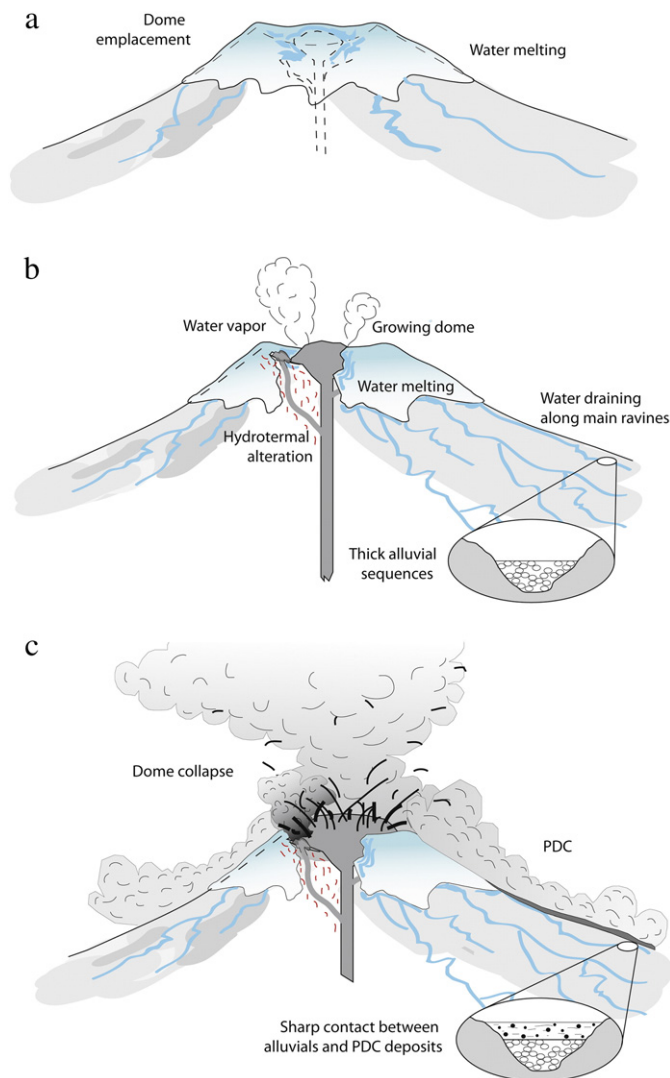
The stratigraphic sections, described in the Cano ravine, show a similar succession of events, but different timings (Fig. 10). Both sections are located along a paleo-valley developed into the PPF, filled at the base by an alluvial succession dominated by conglomerate and fluviatile units directly overlain by BAF deposits. No evidences of time lapse between the alluvial and the pyroclastic activity are visible (Figs. 6 and 8a). Based on available  $^{14}\text{C}$  ages, the calibrated curve of the fluviatile succession precedes and partially overlaps both pyroclastic units representing the two main central dome growth and collapse episodes which occurred at 28  $^{14}\text{C}$  ka and 37  $^{14}\text{C}$  ka (Fig. 10). The climatic record during these periods indicates the existence of a glacier capping the volcano summit and along main valleys (Fig. 4). The summit of the volcano

was then covered by ice when the dome extrusion starts (Fig. 11a). It is also possible that the magmatic intrusion was associated with a strong hydrothermal system promoting glacier melting and high fluid circulation. This has been proposed for the 28 ka event, where the BAF deposit is directly underlain by a debris-avalanche deposit that shows blocks with extensive hydrothermal alteration and evidences of high fluid circulation (Caballero and Capra, 2011; Capra et al., 2013). Subglacial intrusions and the hydrothermal system can promote glacier melting and rapid release of a large amount of water (Major and Newhall, 1989). Under this scenario, it is plausible that during dome growth, and before its collapse, large amount of melting water were drained along main



**Fig. 10.** Calibrated curves of the  $^{14}\text{C}$  ages discussed in the text.





**Fig. 11.** Schematic evolution of the ice-capped Toluca volcano showing the effect of the interaction between the glacier and dome growth, emplacement and collapse. (a) The ice-capped volcano at the initial stage of the dome growth (probably subglacial); (b) dome intrusion, promoting glacier melting and water release along major valleys with the emplacement of fluvial sequences. (c) Gravitational collapse of the dome producing PDCs that directly overlaid the fluvial sequence.

glacial valleys such as at Cano ravine (Fig. 11b). If some phreatic or phreatomagmatic activity preceded the dome collapse is now impossible to be recognized in the stratigraphic record because of the large volume of the emplaced BAFs. The absence of evidences of a depositional gap between the fluvial and the pyroclastic succession points to a sudden collapse of the dome as the fluvial apron was still active (Fig. 11c). At quarry 1 the contact between the fluvial succession and the BAF deposit is horizontal all around the area (Fig. 6), indicating a well-established alluvial fan just prior to the dome collapse. The emplacement of the BAF deposits interrupted the alluvial system that probably deviated to lateral, minor drainages, most likely on the northern sector, where a prominent alluvial fan is recognized (Fig. 2), but no age is available for this sequence. Or, as magmatic activity ceased, the glacier recovered its stability and water discharge drastically decreased. Based on the  $^{14}\text{C}$  data obtained here for the fluvial succession, quarry 1 represents the sequence associated with the 37 ka event and quarry 2 corresponds with the 28 ka episode. In addition, the basal unit of the pyroclastic sequence at section MG09, that erosively overlies the reddish conglomerate and that shows jig-saw features, could correspond to the previously described debris avalanche deposit from a flank collapse

that preceded the 28 ka dome collapse, as already described in the eastern flank of the volcano (Caballero and Capra, 2011) where the edifice instability was accelerated by high fluid circulation (Capra et al., 2013).

## 7. Conclusions

The paleoclimatic reconstruction for the time span studied here is too poor to possibly consider that the magmatic activity related to the 37 ka and 28 ka dome growth is the result of extensive deglaciation inducing decompression and mantle melting (Jull and McKenzie, 1996), or decompression at magma chamber scale with increase on volcanic activity (Huybers and Langmuir, 2009). Instead, the stratigraphic sequence and the moraine extension point to the presence of a glacier on the volcano summit that was disturbed by the intense magmatic and hydrothermal activity related to two dome extrusion episodes. The stratigraphic sequence evidenced an intense fluvial activity in the main glacial valley during the emplacement of the dome. Several examples have been reported in the literature, such as the Nevado del Huila, when on November 20, 2008, a giant lahar inundated part of the Belalcázar town. The day after the event, a dome was spotted on the volcano summit that was thought to have formed during previous months (Smithsonian Institution, 2012). Or the increase in eruptive activity with possible phreatomagmatic eruption was accompanied by lahars at Coaphue volcano (Chile) in 2013 that forced the evacuation of small villages along main valleys (Smithsonian Institution, 2013). So, at ice-capped volcanoes, beside the evaluation of the hazards from magmatic eruptive phases, special attention should be paid to the possible inundation areas from fluvial/lahar activity prior to the main eruption. Even if this is not a possible future scenario for the Nevado de Toluca volcano because of the absence of a glacier nowadays, it represents a clear example for the hazard related to magma–ice interaction in ice-capped volcanoes. The only possible casualty in Mexico could occur at Pico de Orizaba volcano, the only active, ice-capped volcano in Mexico, that already experienced sector collapse in Late Pleistocene (Carrasco-Nuñez et al., 2006; Capra et al., 2013), BAF deposits from summit dome growth during Holocene (Carrasco-Nuñez, 1999), and a dacitic lava flow that descended in the SW flank in historical time.

## Acknowledgments

This work was supported by the DGAPA-UNAM project (IN101213) to Lucia Capra and by a postdoctoral fellowship from DGAPA-UNAM to Lizeth Caballero. The Ministry of Foreign Affairs of Italy and SRE of Mexico provided travel grants to Gianluca Groppelli and Roberto Sulpizio.

## References

- Arce, J.L., Macías, J.L., Vázquez-Selem, L., 2003. The 10.5 ka Plinian eruption of Nevado de Toluca volcano, Mexico: stratigraphy and hazard implications. *Geol. Soc. Am. Bull.* 115, 230–248.
- Arce, J.L., Cervantes, K.E., Macías, J.L., Mora, J.C., 2005. The 12.1 ka Middle Toluca Pumice: a dacitic Plinian–Subplinian eruption of Nevado de Toluca in Central Mexico. *J. Volcanol. Geotherm. Res.* 147, 125–143.
- Bellotti, N., 2004. Evoluzione geologica del Nevado de Toluca (Messico): studio delle interazioni tra edificio vulcanico e tettonica regionale mediante analisi morfologica e modellizzazione analogica. Dipartimento di Scienze della Terra “Ardito Desio”, Università degli Studi di Milano (Honor thesis, 365 pp.).
- Bellotti, N., Capra, L., Groppelli, G., Norini, G., 2006. Tectonic evolution of the Toluca Basin and its influence on the eruptive history of the Nevado de Toluca volcano. *J. Volcanol. Geotherm. Res.* 158, 21–36.
- Benn, D.I., Hulton, N.R.J., 2010. An Excel spreadsheet program for reconstructing the surface profile of former mountain glacier and ice caps. *Comput. Geosci.* 36, 605–610.
- Brock, B., Rivera, A., Casassa, G., Bown, F., Acuna, C., 2007. The surface energy balance of an active ice-covered volcano: Villarica Volcano, Southern Chile. *Ann. Glaciol.* 45, 104–114.
- Caballero, L., Capra, L., 2011. Textural analysis of particles from El Zaguán debris avalanche deposit, Nevado de Toluca volcano, Mexico: evidence of flow behavior during emplacement. *J. Volcanol. Geotherm. Res.* 200, 75–82.

- Caballero, M., Macías, J.L., Urrutia-Fucugauchi, J., Lozano-García, S., Castañeda, R., 2000. Volcanic stratigraphy and palaeolimnology of the Upper Lerma Basin during Late Pleistocene and Holocene. *Sedimentology* 30, 57–71.
- Calvari, S., Tanner, L.H., Groppelli, G., Norini, G., 2004. A comprehensive model for the opening of the Valle del Bove depression and hazard evaluation for the eastern flank of Etna volcano. In: Bonaccorso, A., et al. (Eds.), *Mt. Etna: Volcano Laboratory*. AGU Geophysical Monograph Series 143, pp. 65–75.
- Capra, L., Norini, G., Groppelli, G., Macías, J.L., Arce, J.L., 2008. Volcanic hazard zonation of the Nevado de Toluca volcano, México. *J. Volcanol. Geotherm. Res.* 176, 469–484.
- Capra, L., Bernal, J.P., Carrasco-Núñez, G., Roverato, M., 2013. The climatic fluctuations as a significant contributing factor for volcanic collapses. Evidence from Mexico during the Late Pleistocene. *Glob. Planet. Chang.* 100, 194–203.
- Carrasco-Núñez, G., 1999. Holocene block-and-ash flows from summit dome activity of Citlaltépetl volcano, Eastern Mexico. *J. Volcanol. Geotherm. Res.* 88, 47–66.
- Carrasco-Núñez, G., Díaz-Castellón, R., Siebert, L., Hubbard, B., Sheridan, M.F., Rodríguez-Elizarrarás, S.R., 2006. Multiple edifice-collapse events in the Eastern Mexican Volcanic Belt: the role of sloping substrate and implication for hazard assessment. *J. Volcanol. Geotherm. Res.* 158, 151–176.
- D'Antonio, M., Capra, L., Sarocchi, D., Bellotti, N., 2008. Reconstrucción del evento eruptivo asociado al emplazamiento del flujo piroclástico El Refugio hace 13 ka volcán Nevado de Toluca (México). *Rev. Mex. Cienc. Geol.* 25, 115–134.
- García-Palomo, A., Macías, J.L., Arce, J.L., Capra, L., Espíndola, J.M., Garduno, V.H., 2002. Geology of Nevado de Toluca volcano and surrounding areas, central Mexico. *Geological Society of America Map and Chart Series*. MCH089.
- Guðmundsson, M.T., Sigmundsson, F., Björnsson, H., 1996. Ice-volcano interaction of the 1996 Gjálp subglacial eruption. *Vatnajökull, Iceland. Nature* 389 (1997), 954–957.
- Heine, K., 1988. Late quaternary glacial chronology of the Mexican volcanoes. *Geowissenschaften* 6, 197–205.
- Heine, K., 1994. Present and past geocryogenic processes in Mexico. *Permafrost. Periglacial Process.* 5, 1–12.
- Huybers, P., Langmuir, C., 2009. Feedback between deglaciation, volcanism, and atmospheric CO<sub>2</sub>. *Earth Planet. Sci. Lett.* 286, 479–491.
- Julio-Miranda, P., Delgado, H., Huggel, C., Kaab, A., 2008. Impact of the eruptive activity on glacier evolution at Popoactépetl Volcano (México) during 1994–2004. *J. Volcanol. Geotherm. Res.* 170, 86–98.
- Jull, M., McKenzie, D.P., 1996. The effect of deglaciation on mantle melting beneath Iceland. *J. Geophys. Res.* 101 (21), 815–828.
- Kaplan, M.R., Moreno, P., Rojas, M., 2008. Glacial dynamics in southernmost South America during Marine Isotope Stage 5e to the Younger Dryas chron: a brief review with a focus on cosmogenic nuclide measurements. *J. Quat. Sci.* 23 (6–7), 649–658.
- Macías, J.L., García-Palomo, A., Arce, J.L., Siebe, C., Espíndola, J.M., Komorowski, J.C., Scott, K.M., 1997. Late Pleistocene–Holocene cataclysmic eruptions at Nevado de Toluca and Jocotitlán Volcanoes, Central Mexico. In: Kowallis, B.J. (Ed.), *Proterozoic to Recent Stratigraphy, Tectonics, and Volcanology, Utah, Nevada, Southern Idaho and Central Mexico*. BYU Geology Studies, pp. 493–528.
- Major, J., Newhall, C., 1989. Snow and ice perturbation during historical volcanic eruptions and the formation of lahar and floods. *Bull. Volcanol.* 52, 1–27.
- Metcalfe, S.E., Street-Perrott, A., Perrott, A., Harkness, D.D., 1991. Palaeolimnology of the Upper Lerma Basin, Central Mexico: a record of climatic change and anthropogenic disturbance since 11600 yr BP. *J. Paleolimnol.* 5, 197–218.
- Mitasova, H., Hofierka, L., 1993. Interpolation by regularized spline with tension: II. Application to terrain modeling and surface geometry analysis. *Math. Geol.* 25, 657–669.
- Mitasova, H., Mitas, L., 1993. Interpolation by regularized spline with tension: I. Theory and implementation. *Math. Geol.* 25, 641–655.
- Norini, G., 2006. Relazioni tra attività tettonica e vulcanismo: evidenze e modelli dallo studio del vulcano Nevado de Toluca (Messico). Dipartimento di Scienze della Terra “Ardito desio”, Università degli Studi di Milano, p. 268 (PhD Thesis).
- Norini, G., Capra, L., Groppelli, G., Lagmay, A.M.F., 2008. Quaternary sector collapses of Nevado de Toluca volcano (Mexico) as consequence of regional tectonics and volcanic evolution. *Geosphere* 4 (5), 854–871.
- Norini, G., Capra, L., Groppelli, G., Agliardi, F., Pola, A., Cortes, A., 2010. Structural architecture of the Colima Volcanic Complex. *J. Geophys. Res. Solid Earth* 115, B12209–B12220.
- Pierson, T.C., Janda, R.J., Thouret, J.C., Borrero, C.A., 1990. Perturbation and melting of snow and ice by the 13 November 1985 eruption of Nevadode Ruiz, Colombia, and consequent mobilization, flow and deposition of lahars. *J. Volcanol. Geotherm. Res.* 41, 17–66.
- Reimer, P.J., Baillie, M.G.L., Bard, E., Bayliss, A., Beck, J.W., Bertrand, C.J.H., Blackwell, P.G., Buck, C.E., Burr, G.S., Cutler, K.B., Damon, P.E., Edwards, R.L., Fairbanks, R.G., Friedrich, M., Guilderson, T.P., Hogg, A.G., Hughen, K.A., Kromer, B., McCormac, F.G., Manning, S.W., Ramsey, C.B., Reimer, R.W., Remmele, S., Southon, J.R., Stuiver, M., Talamo, S., Taylor, F.W., van der Plicht, J., Weyhenmeyer, C.E., 2004. IntCal04 Terrestrial radiocarbon age calibration, 26–0 ka BP. *Radiocarbon* 46, 1029–1058.
- Rivera, A., Bown, F., Mella, R., Wendt, J., Casassa, G., Acuña, C., Rignot, E., Clavero, J.E., Brock, B., 2006. Ice volumetric changes on active volcanoes in Southern Chile. *Ann. Glaciol.* 43, 111–122.
- Smithsonian Institution, 2012. Nevado del Huila. *Bull. Global Volcanism Net.* 37, 10.
- Smithsonian Institution, 2013. Copahue. *Bull. Global Volcanism Net.* 38, 09.
- Solleiro-Rebollero, E., Macías, J.L., Gama Castro, J.E., Sedov, S., Sulerzhitsky, L.D., 2004. Quaternary pedostratigraphy of the Nevado de Toluca volcano. *Rev. Mex. Cienc. Geol.* 21, 101–109.
- Stuiver, M., Reimer, P.J., 1993. Extended 14C database and revised CALIB radiocarbon calibration program. *Radiocarbon* 35, 215–230.
- Thackray, G.D., Staley, A.E., 2014. Extensive glaciation during MIS 4 and 3 in the Teton range, Wyoming. *Rocky Mountain (66th Annual) and Cordilleran (110th Annual) Joint Meeting (19–21 May 2014)*, Abstract 29–4.
- Thorpe, P.W., 1991. Surface profiles and basal shear stresses of outlet glacier from a Late-Glacial mountain ice field in western Scotland. *J. Glaciol.* 37, 78–88.
- Torres-Orozco, R., 2012. Volcanismo efusivo en el área del Nevado de Toluca: distribución y génesis de magma. Instituto de Geología, Universidad Nacional Autónoma de México, Mexico D.F (Master Thesis, 138 pp.).
- Tuffen, H., 2010. How will melting of ice affect volcanic hazards in the twenty-first century? *Philos. Trans. R. Soc. Lond.* 368, 2535–2558.
- Vázquez-Selem, L., Heine, K., 2011. Late quaternary glaciation in Mexico. In: Ehlers, J., Gibbard, P.L., Hughes, P.D. (Eds.), *Quaternary Glaciations – Extent and Chronology*. Elsevier B.V., pp. 849–861.
- Wadge, G., Francis, P.W., Ramirez, C.F., 1995. The Socompa collapse and avalanche event. *J. Volcanol. Geotherm. Res.* 66, 309–336.
- Williams, S.N., 1987. Nevado del Ruiz volcano, Colombia: the November 1985 eruption and related events. *J. Volcanol. Geotherm. Res.* 1987, 355–360.